

Optimization and Performance Analysis of a $\text{TiO}_2/\text{i-CH}_3\text{NH}_3\text{SnBr}_3/\text{CsPbI}_3/\text{Al(BSF)}$ Heterojunction Perovskite Solar Cell for Enhanced Efficiency

Mohamed Ghaleb, Amina Arrar,* and Zaza Touaa



Cite This: *ACS Omega* 2023, 8, 37011–37022

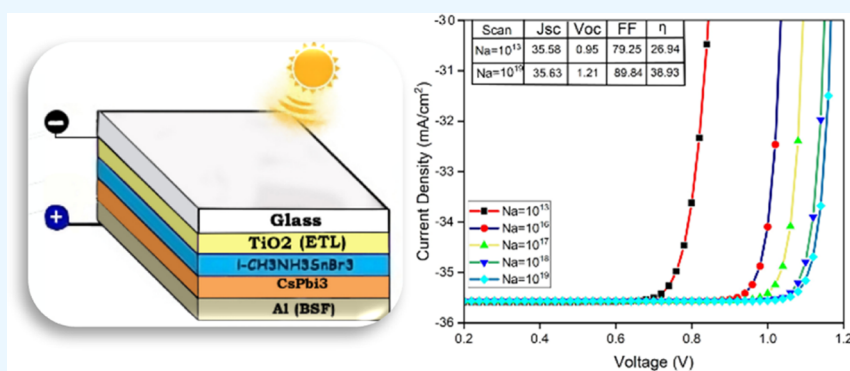


Read Online

ACCESS |

Metrics & More

Article Recommendations



ABSTRACT: This paper reports the simulation and optimization of heterojunction perovskite solar cells (PSCs) with a proposed structure of $\text{TiO}_2/\text{i-CH}_3\text{NH}_3\text{SnBr}_3/\text{CsPbI}_3/\text{Al(BSF)}$ using SCAPS-1D software. The purpose of this study is to investigate the performance of the PSC with CsPbI_3 perovskite active layers and $\text{i-CH}_3\text{NH}_3\text{SnBr}_3$ as the permeable layer. Therefore, the thicknesses of the layers of the heterojunction perovskite are modified in order to find a better conversion efficiency of the solar cell, where the latter's performance is improved by optimizing the absorber's thickness, which is found to be $1 \mu\text{m}$, with a permeable layer of $15 \mu\text{m}$. The device efficiency of the $\text{i-CH}_3\text{NH}_3\text{SnBr}_3/\text{CsPbI}_3$ heterojunction is improved to 38.98%, and optimized parameters are $V_{oc} = 1.21 \text{ mV}$, $J_{sc} = 35.63 \text{ mA/cm}^2$, and $\text{FF} = 89.84\%$. The acceptor concentration (N_a), donor concentration (N_d), defect density, and series and shunt resistances are also investigated.

1. INTRODUCTION

The search for efficient and low-cost renewable energy sources is of great importance in the modern world. As conventional fossil fuel sources of electricity became scarcer and cause severe problems for our planet's climate, it becomes increasingly imperative to seek new and innovative ways of exploiting sustainable resources.¹

However, converting light energy into electrical energy is not an absolute process; there are losses that affect the performance of photovoltaic cells due to the nature of the material and technology used.

In recent years, there has been immense interest in heterojunction perovskite solar cells (PSCs), particularly when the power conversion efficiency (PCE) of organic–inorganic perovskite solar cells has increased from 3.8 to 26%.^{2–4} The perovskite material may be used alone as an absorber in different solar device designs and architectures, but it can also be utilized in conjunction with the standard silicon layer to lower the \$/W value.⁵

This significant improvement has been made possible due to the excellent optoelectronic characteristics of halide perovskite materials used including their high absorption coefficient, low exciton binding energies, long-range charge diffusion lengths, acceptable band gaps, and high charge carrier mobilities.⁶

In this work, we propose aluminum (Al) as a back-surface field (BSF) layer and work with two types of perovskites. The BSF has been used as a way to increase solar cell performance by reducing the surface recombination velocity (SRV). It is also a region at the rear surface of a solar cell that is more doped than the surrounding area. The interface between the high- and low-doped regions acts like a p–n junction, creating an electric field that presents a barrier to the flow of minority carriers to the rear

Received: June 19, 2023

Accepted: September 8, 2023

Published: September 27, 2023



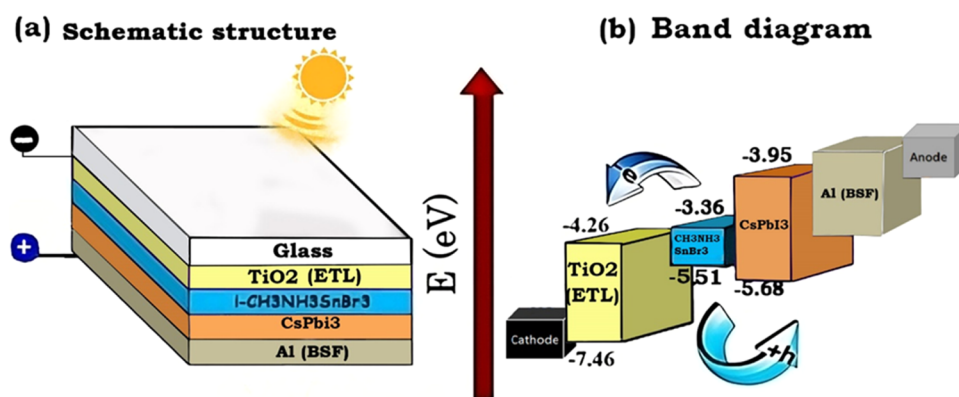


Figure 1. (a) Simple schematic structure view and (b) energy level diagram of the glass/TiO₂/i-CH₃NH₃SnBr₃/CsPbI₃/Al(BSF) heterojunction solar cell.

surface. This maintains the minority carrier concentration in the bulk of the device at higher levels and has a passivating net effect on the rear surface.⁷ i-CH₃NH₃SnBr₃, which belongs to the hybrid halide perovskite p-type belongs to the class of semiconductors with the general formula ABX₃, in which the metal cation B is Sn²⁺ at the center, X represents a monovalent anion Br⁻, and A is a monovalent cation such as the organic molecular [CH₃NH₃]⁺, chosen to neutralize the overall charge.⁸ Additionally, the organic–inorganic halide perovskite solar cells (PSCs) have gained substantial attention in the past decade and are expected to compete with conventional silicon-based solar cells due to their outstanding device performance.⁷ Among the inorganic halide perovskites, CsPbI₃ has been reported to show higher thermal stability,⁹ especially in the cubic phase, which exhibits the most suitable band gap of 1.694 eV for photovoltaic applications.^{10,11} From 2015 until now, the device efficiency for CsPbI₃ has increased from 2.9%^{10,12} to 19.03%¹³ and to 21.75% by the group of Shengzhong (Frank) Liu¹⁴ indicating its great potential for high-efficiency inorganic PSCs. TiO₂, a wide band gap ($E_g = 3.2$ eV) n-type semiconductor with high electron affinity, has been successfully used in perovskite and dye-sensitized solar cells.^{15,16} It is commonly used as an electron transport layer (ETL) in various types of solar cells including perovskite solar cells and dye-sensitized solar cells (DSSCs). It provides a favorable energy level alignment for efficient charge extraction and helps to prevent the recombination of electron–hole pairs. The combination of TiO₂ with its unique properties and its compatibility with other materials makes it a widely used and successful component in perovskite solar cells.^{15,16}

The photovoltaic performance parameters of the proposed structure TiO₂/i-CH₃NH₃SnBr₃/CsPbI₃/Al (BSF) heterojunction thin film with BSF were determined using numerical analysis utilizing SCAPS-1D software. The investigation of the influence of the thickness, PCE, temperature, quantum efficiency (QE), open-circuit voltage, fill factor, short-circuit current density with varying N_a and N_D , series and shunt resistances, and defect density was carried out for solar cells. The results showed that the proposed PSC structure with CsPbI₃ as the perovskite active layer and i-CH₃NH₃SnBr₃ as the permeable layer could achieve a maximum PCE of 38.98%. Many simulations were performed to determine the theoretical PCE of CH₃NH₃SnBr₃ and CsPbI₃ solar cells. Md. Samiul Islam et al. achieved 21.66% efficiency for the ITO/TiO₂/CH₃NH₃SnBr₃/NiO solar device layer using SCAPS-1D.¹⁷ Duan et al. achieved 18.29% efficiency for the FTO/TiO₂/

CH₃NH₃PbI₃/carbon using wxAMPS software,¹⁸ and more comparative results are given in Table 6.

2. THEORY AND METHODS

The numerical simulation of solar cells is used by SCAPS-1D, which was programmed by Burgelman at the University of Ghent, Belgium.¹⁹ The proposed heterojunction used in this work is depicted in Figure 1. It consists of TiO₂/i-CH₃NH₃SnBr₃/CsPbI₃/Al (BSF). The structure includes TiO₂ with a band gap of 3.2 eV as the window layer, the permeable absorption layer i-CH₃NH₃SnBr₃, and the absorption layer CsPbI₃ perovskite. Additionally, Al is used as a back-contact BSF layer. Glass substrates are employed in the processing of these materials to increase the efficiency and transparency. The contact parameters are depicted in Table 1.

Table 1. Left and Right Contact Parameters (Thermionic Emission/Surface Recombination Velocity)

parameters	left contact (back)	right contact (front)
electrons (cm/s)	10 ⁵	10 ⁷
holes (cm/s)	10 ⁷	10 ⁵

It is a freely available program based on Poisson's equation as following²⁰

$$\nabla(E) = \frac{q}{\epsilon}(p - n + N_D^+ - N_A^-) \quad (1)$$

where E is the electrical field, q is the electron charge, ϵ is the permittivity of the absorber, n is the density of electrons, p is density of holes, N_D is the donor concentration, and N_A is the acceptor concentration.

The continuity equations can be obtained from the following equations^{20,21}

$$\frac{dn}{dt} = \frac{1}{q}(\nabla(J_n) + G_n - R_n) \quad (2)$$

$$\frac{dp}{dt} = -\frac{1}{q}(\nabla(J_p) + G_p - R_p) \quad (3)$$

where G_n is the electron generation rate, G_p is the hole generation rate, J_n is the electron current density, J_p is the hole current density, R_n is the electron recombination rate, and R_p is the hole recombination rate.

The charge carrier equations for diffusion and drift current can be obtained from the following equations^{21,22}

Table 2. Regrouping of the Physical Parameters Employed in Our Simulation

	Al-BSF	CsPbI ₃	i-CH ₃ NH ₃ SnBr ₃	TiO ₂
layer thickness (μm)	0.050	varied	varied	0.100
dielectric constant dk	11.9	6	10	9
band gap eg (ev)	1.12	1.694	1.3	3.20
electron affinity chi (ev)	4.05	3.95	4.17	4
effective conduction band density (cm^{-3})	2.8×10^{19}	1.1×10^{20}	2.2×10^{18}	1×10^{21}
effective valence band density (cm^{-3})	1.04×10^{19}	8.2×10^{20}	1.8×10^{18}	2×10^{20}
electron mobility ($\text{cm}^2 \text{v}^{-1} \text{s}^{-1}$)	202.4	25	1.6	20
hole mobility ($\text{cm}^2 \text{v}^{-1} \text{s}^{-1}$)	5	25	1.6	10
doping concentration of donators (cm^{-3})	0	0	1×10^{13}	1×10^{18}
doping concentration of acceptors (cm^{-3})	1×10^{20}	1×10^{15}	1×10^{13}	0
thermal velocity of electron ($\text{cm}^{-3} \text{s}^{-3}$)	1×10^7	1×10^7	1×10^7	1×10^7
thermal velocity of holes ($\text{cm}^{-3} \text{s}^{-3}$)	1×10^7	1×10^7	1×10^7	1×10^7
auger recombination coefficient for electron ($\text{cm}^6 \text{s}^{-1}$)	$2.2 \cdot 10^{-31}$	$2.2 \cdot 10^{-31}$		
auger recombination coefficient for hole ($\text{cm}^6 \text{s}^{-1}$)	$9.9 \cdot 10^{-32}$	$9.9 \cdot 10^{-32}$		
references	24	25	17	26,27

$$J_n = q(\mu_n n E + D_n \nabla n) \quad (4)$$

$$J_p = q(\mu_p p E + D_p \nabla p) \quad (5)$$

The fill factor percent (FF) can be expressed by the following equation²¹

$$\text{FF} = \frac{P_{\text{max}}}{P_{\text{in}}} = \frac{V_{\text{max}} \cdot I_{\text{max}}}{V_{\text{oc}} \cdot J_{\text{sc}}} \quad (6)$$

The energy conversion efficiency percent (PCE%) of a thin film can be expressed by eq 7:^{20,23}

$$\text{PCE}\% = \frac{P_m}{P_{\text{in}}} = \frac{V_{\text{oc}} \cdot J_{\text{sc}} \cdot \text{FF}\%}{P_{\text{in}}} \quad (7)$$

$$V_{\text{oc}} = \frac{KT}{q} \ln \left[\frac{J_{\text{sc}}}{J_0} + 1 \right] \quad (8)$$

That V_{oc} is a function of both J_{sc} and the saturation current density of the device J_0 , which depends also on the thickness of the layer.

In this simulation, several parameters and conditions were taken into account. The thermal velocity of electrons and holes used in the simulation was 107 cm/s. This parameter represents the average velocity of charge carriers (electrons and holes) due to the thermal energy at a given temperature. The standard photovoltaic radiation spectrum AM 1.5 G was employed, which represents the solar spectrum under terrestrial conditions. It has a power density of 1000 W/m² and a temperature of 300 K. This spectrum is widely used in photovoltaic simulations to evaluate the performance of solar cells. Table 2 regroupes the physical parameters employed in our simulation.

3. RESULTS AND DISCUSSION

3.1. Optimization of Absorber Layer Thickness.

Optimizing the absorber layer thickness is an essential step in the development of high-performance solar cells. The absorber layer, also known as the perovskite layer in this case, is responsible for absorbing sunlight and converting it into electrical energy. The thickness of this layer directly affects the amount of sunlight that is absorbed and converted to electrical energy, which ultimately affects the device's performance.

In this study, the researchers aimed to optimize the thickness of the absorber perovskite layer CsPbI₃ and the preamble layer i-

CH₃NH₃SnBr₃ to achieve maximum power conversion efficiency (PCE) of the device.

To accomplish this, they varied the thicknesses from 1.0 to 15.0 μm . The thicknesses of the window and back layers remained fixed at their initial values, while the thickness of the i-CH₃NH₃SnBr₃ layer first varied from 1.0 to 15.0 μm , followed by changes in the CsPbI₃ layer thickness. Once the optimal thickness was determined, it was used for the remaining simulation.

The results showed that the PCE of the device increased as the absorber layer thickness increased, peaking at 31.95% for an absorber layer thickness of 15.0 μm . This highlights the importance of optimizing the thickness of the absorber layer, as it significantly affects the performance of the device.

Figure 2a,b illustrates the effect of layer thickness on the device's power conversion efficiency (PCE) (%) for all layers. It is noteworthy that as the thickness of the CsPbI₃ layer increases, the efficiency slightly improves from 28.80 to 31.19%, with maximum achievable photovoltaic parameters of FF = 87.67%, $J_{\text{sc}} = 34.78 \text{ mA/cm}^2$, and $V_{\text{oc}} = 1.02 \text{ V}$.

Similarly, as the thickness of the i-CH₃NH₃SnBr₃ layer increases, the efficiency increases from 31.19 to 31.95%, with maximum achievable photovoltaic parameters of PCE = 31.95%, FF = 86.76%, $J_{\text{sc}} = 35.56 \text{ mA/cm}^2$, and $V_{\text{oc}} = 1.03 \text{ V}$.

Figure 3a,b illustrates the changes in the photovoltaic parameters of the double-layer absorber materials when the thickness of the bromine-doped tin perovskite absorber layer has varied from 1.0 to 15.0 μm , while the preamble layer thickness is kept constant at 15 μm . As the thickness of the absorber layer increases, the photovoltaic parameters also increase. The optimal values for PCE, FF, J_{sc} , and V_{oc} were found to be 31.95%, 86.76%, 35.56 mA/cm², and 1.03 V respectively. Therefore, the device configuration and selected materials are reasonable to a certain extent. Further research can be conducted based on this model.

These graphs revealed that the best thicknesses for the absorber and the permeable layers are fixed at 1 and 15 μm , respectively, because a high PCE is given at these thicknesses.

3.2. Improvement in Cell Performance. The performance of these simulated PSCs was studied by obtaining their short-circuit photocurrent density vs voltage (J - V) curve. Figure 4 shows simulated J - V characteristics of CsPbI₃ calculated with the physical parameters in Table 2. The J - V results indicate an interesting PCE of 31.95% for CsPbI₃ layer-

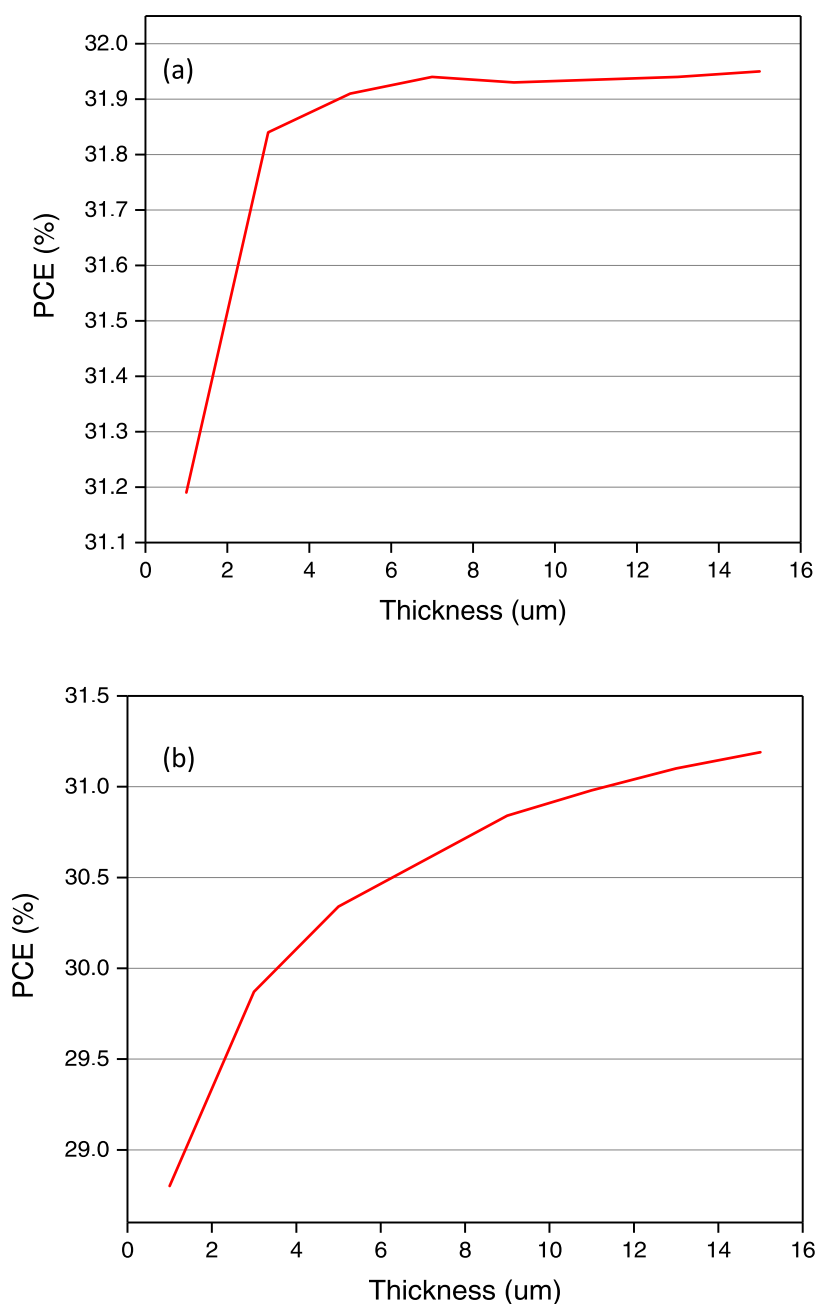


Figure 2. Effect of (a) $i\text{-CH}_3\text{NH}_3\text{SnBr}_3$ and (b) CsPbI_3 layer thickness on PCE.

based PSCs at 300 K. The simulated PSCs also exhibit an excellent V_{oc} of 1.03 V with J_{sc} of 35.56 and 8.11 mA/cm^2 and FF = 86.76%. We can see that the J_{sc} values increase from -35.53 to -21.58 mA/cm^2 and the V_{oc} increases from 0 to 1.0 V.

The spectral response has been evaluated based on the quantum efficiency measurements. QE is defined according to the following equation²²

$$QE(\lambda) = \frac{\text{number of collected electrons}}{\text{number of incident photons}} = \frac{I(\lambda)/q}{Q_p(\lambda)} \quad (9)$$

where q is the elementary electrical charge, $I(\lambda)$ is the photogenerated current, and $Q_p(\lambda)$ is the photon flow.

The quantum efficiency (QE%) is shown in Figure 5 under AM 1.5 G (1000 W m^{-2} , 300 K) illumination of the device with the optimized simulated parameters. The optimized parameters

of the device are as follows: a $1 \mu\text{m}$ CsPbI_3 thin layer and a $15 \mu\text{m}$ $i\text{-CH}_3\text{NH}_3\text{SnBr}_3$ thin layer, 10^{15} cm^{-3} shallow acceptor density of the absorber layer, donor and acceptor defects of 10^{13} cm^{-3} concentration in the absorber layer, and a neutral interface defect of 10^{13} cm^{-3} . The simulated device achieves a QE of 55% at a wavelength of 150 nm. After that, the QE reaches 100% in the wavelength range of 400 nm to 950 nm. It is possible that the absence of consideration for the surface and interface reflectance in this simulation contributes to this result. However, beyond 950 nm, the QE starts to decrease.

3.3. Optimization of Parameters of the n-Type TiO_2 Layer. In this section, we conducted simulations on the parameters of the TiO_2 layer. Figure 6(a) illustrates the J - V curves while the donor concentration is varied from 10^{15} to 10^{21} cm^{-3} . The variations of photovoltaic parameters, namely, V_{oc} , J_{sc} , FF, and efficiency (PCE%), are depicted in Figure 6b,c. As the

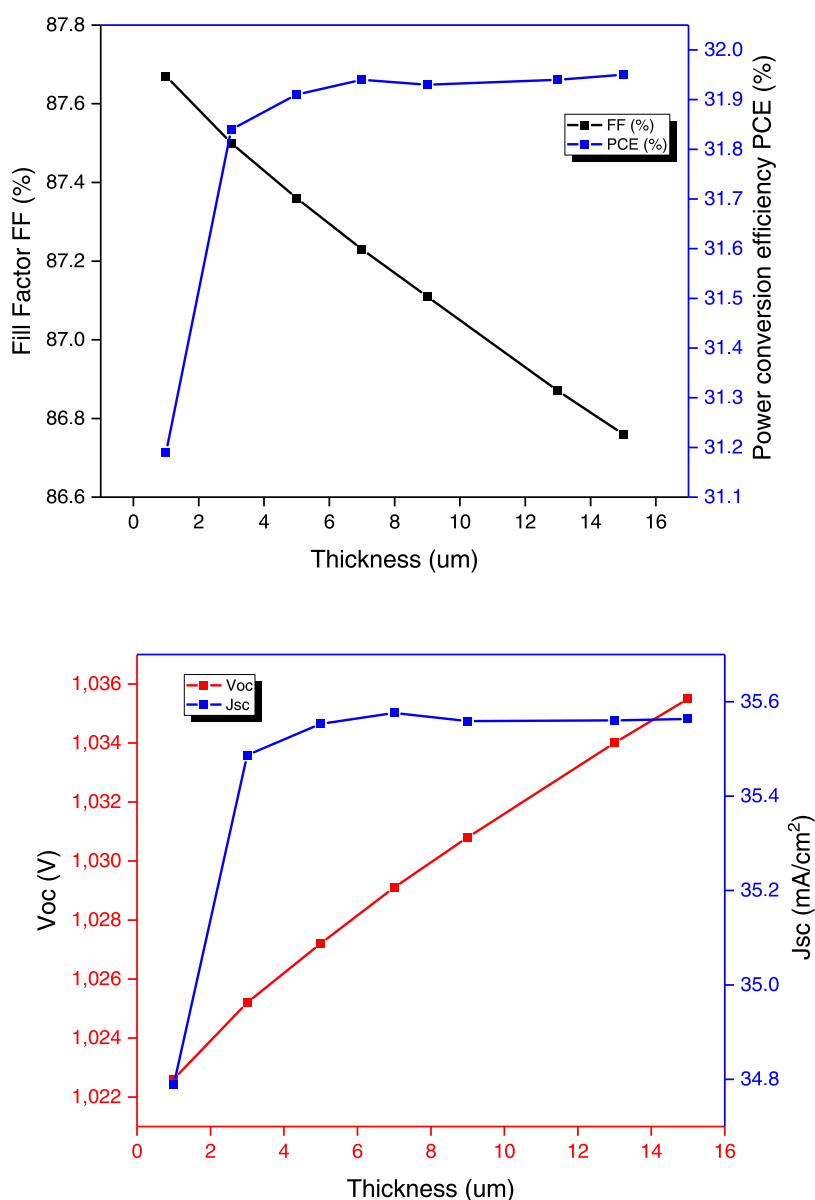


Figure 3. Graph representing the variation of PV parameters with the thickness of the absorber layer.

donor concentration (N_d) increases from 10^{16} to 10^{21} cm^{-3} , it is observed that FF and V_{oc} increase, while efficiency and J_{sc} decrease, particularly when the N_d of the perovskite layers reaches around 10^{16} cm^{-3} . This behavior is attributed to the increase in conductivity with a higher donor concentration. The optimal results for all PV parameters are obtained when N_D is set at 10^{21} cm^{-3} . At this doping concentration 10^{16} cm^{-3} , the maximum power conversion efficiency is 32.01% with FF = 83.85%, J_{sc} = 34.65 mA/cm^2 , and V_{oc} = 1.18 V.

3.4. Optimization of Parameters of the p-Type CsPbI₃ Layer. The second step involved studying the impact of the acceptor concentration (N_a) in the perovskite absorbing layer on the J - V characteristics of the solar cells, as shown in Figure 7a. Following optimization, the J - V curve shifts toward higher values of V_{oc} and J_{sc} . Upon observing the graphs in Figure 7b,c, it is evident that all photovoltaic parameters, including PCE, FF, J_{sc} , and V_{oc} , increase from 10^{15} to 10^{19} cm^{-3} . Specifically, the optimized values for FF, J_{sc} , V_{oc} , and PCE are found to be 89.84%, 35.63 mA/cm^2 , 1.21 V, and 38.93%, respectively. These values represent improvements over the initial parameters.

3.5. Effect of Temperature. Temperature changes can have a significant impact on the fill factor (FF) percentage, power conversion efficiency (PCE), and overall performance of the device.²⁸ The fill factor represents the efficiency of a solar cell by considering the maximum power output it can deliver compared to the product of the open-circuit voltage (V_{oc}) and short-circuit current (I_{sc}). As temperature increases, the FF percentage tends to decrease due to the increase in defect density within the layers.²⁹ This increase in defect density leads to a decrease in charge carrier mobility and recombination, ultimately reducing the FF percentage.

Furthermore, the power conversion efficiency (PCE) of the device is also affected by temperature variations. The PCE is a measure of how effectively the solar cell converts incident light into electrical energy. As the temperature increases, the increase in defect density further hampers charge carrier transport, leading to decreased PCE. The reduction in PCE can be attributed to increased resistive losses and enhanced recombination processes within the device.

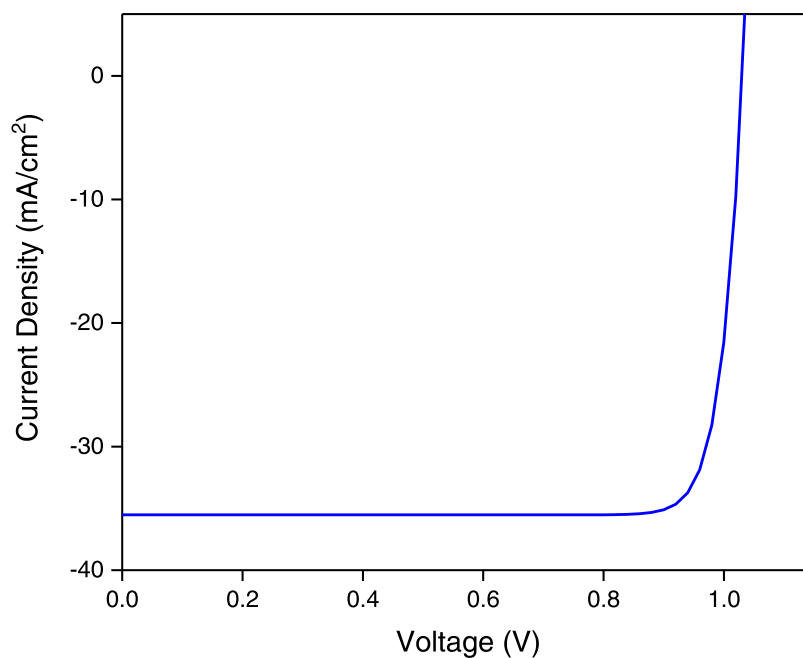


Figure 4. Simulated J - V characteristics of CsPbI₃.

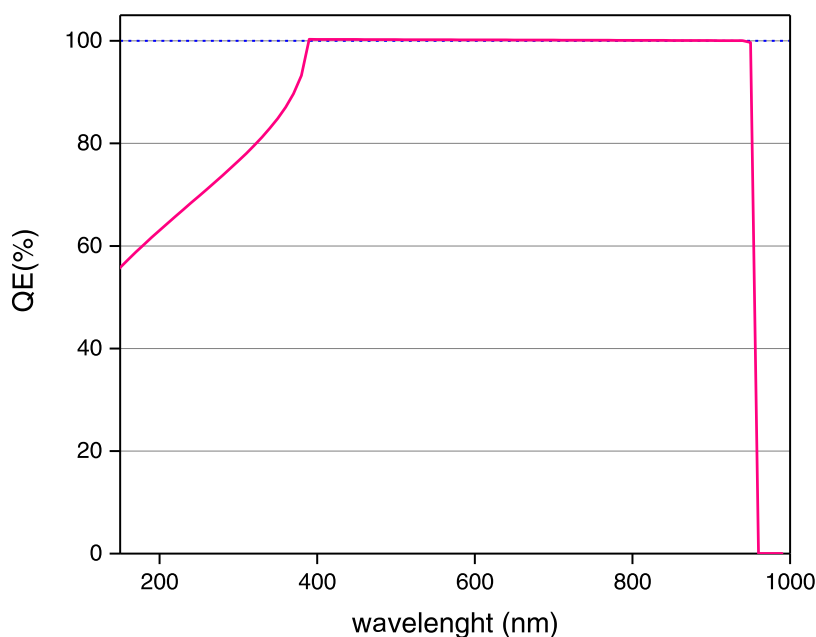


Figure 5. Quantum efficiency of the PSC.

From Figure 8, it can be observed that with increasing temperature, the FF percentage decreases, and the device efficiency diminishes. The maximum efficiency rate achieved is 35.40%. However, it is noteworthy that at lower temperatures below 280 K, the performance of the solar cell improves significantly, reaching a higher efficiency value of 35.58%. This improvement can be attributed to the reduced defect density and enhanced charge carrier mobility, resulting in lower recombination rates and improved overall device performance.

3.6. Impact of Series and Shunt Resistances. Now, we will investigate the effect of series and shunt resistance; the chain's resistance will be increased from 1 to 5 $\Omega\cdot\text{cm}^2$, while the shunt resistance will change from $1 \times 10^1 \Omega\cdot\text{cm}^2$ to $1 \times 10^7 \Omega\cdot\text{cm}^2$. The results are shown in Tables 3 and 4.

Table 3, it has been observed that the increase in series resistance adversely affects the fill factor, and once R_s is remarkably high, it slightly affects the J_{sc} . These findings are completely in agreement with those reported in the literature. It has been observed that FF degrades almost 3.7% with each 1 $\Omega\cdot\text{cm}^2$ increase in R_s , which is a little higher than the conventional Si solar cell.

However, while FF degrades at 3.6%, efficiency degrades at a much lower rate; only at 1.6% with 1 $\Omega\cdot\text{cm}^2$, we notice an increase in R_s , while the rest of the parameters have not changed (J_{sc} , V_{oc}).

The shunt resistance represents any parallel high conductivity paths (shunts) across the solar cell p-n junction or on the cell edges. These are due to the crystal scratches and impurities in

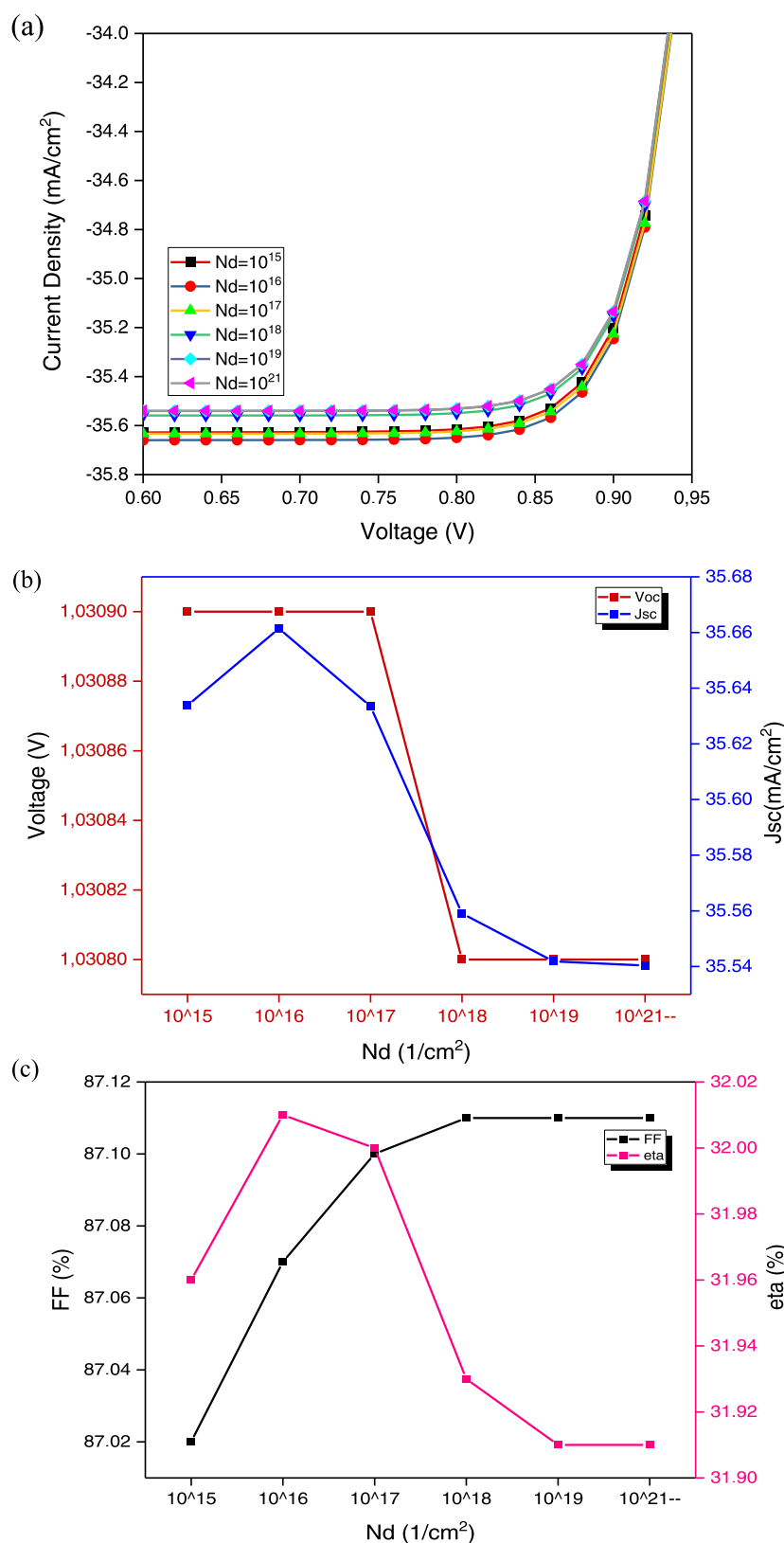


Figure 6. (a) $J-V$ curves obtained by the optimization of donor concentration (N_d) of heterojunction solar cells. (b) Change trend of V_{oc} and J_{sc} . (c) Change Trend of FF and PCE %.

and near the junction and rise of the shunt current. Shunt paths lead the current away from the intentional load, and their effects are detrimental to the module performance mainly at low intensity levels.³⁰

Table 4 presents the outcome of the variation in shunt resistance (R_{sh}) within the range of $1 \times 10^1 \Omega \cdot \text{cm}^2$ to $1 \times 10^7 \Omega \cdot \text{cm}^2$ and its impact on several crucial parameters of the solar cell's performance. The investigated parameters include the

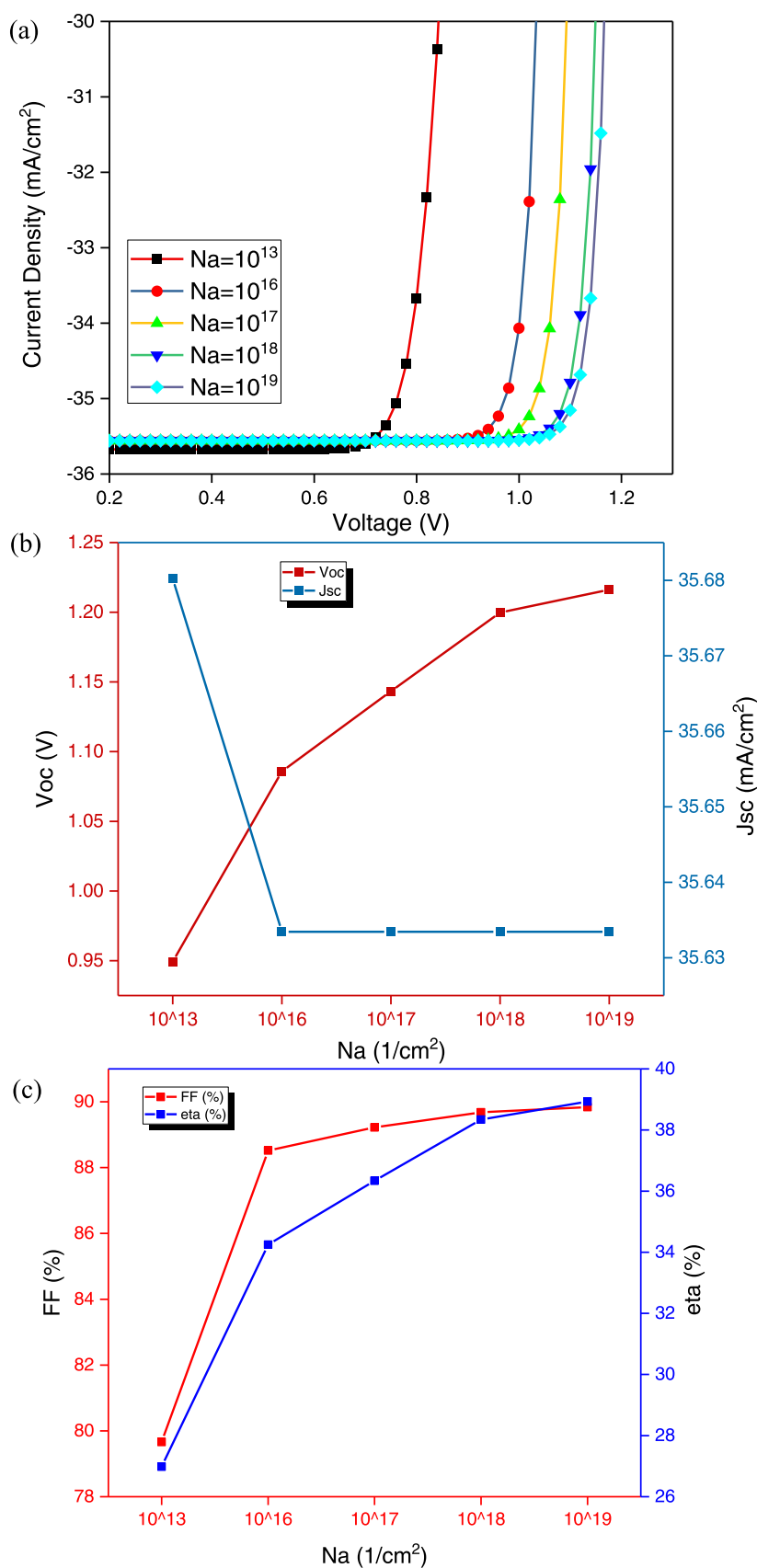


Figure 7. (a) $J-V$ curves obtained by the optimization of acceptor concentration (N_a) of heterojunction solar cells. (b) Change trend of V_{oc} and J_{sc} . (c) Change trend of FF and PCE %.

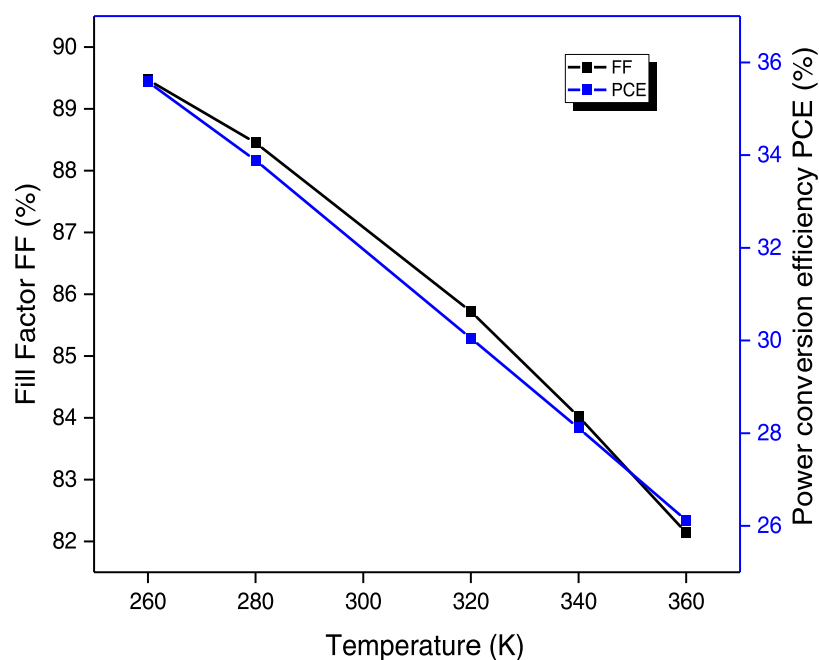


Figure 8. Variation of efficiency and fill factor with the temperature (K).

Table 3. Effect of Series Resistance Changes on $\text{CH}_3\text{NH}_3\text{SnBr}_3/\text{CsPbI}_3$

resistance ($\Omega\cdot\text{cm}^2$)	PCE (%)	FF	J_{sc}	V_{oc}
0	31.95	86.76	35.563395	1.0466
1	28.42	80.93	35.564105	0.9873
2	27.24	77.59	35.564100	0.9874
3	26.08	74.27	35.564096	0.9874
4	24.95	71.03	35.564092	0.9875
5	23.80	67.78	35.564087	0.9875

Table 4. Effect of Shunt Resistance Changes on $\text{CH}_3\text{NH}_3\text{SnBr}_3/\text{CsPbI}_3$

R_{sh} ($\Omega\cdot\text{cm}^2$)	PCE	FF	J_{sc}	V_{oc}
1×10^1	3.16	25.00	35.564109	0.3556
1×10^2	29.60	84.32	35.564109	0.9871
1×10^3	29.60	84.32	35.564109	0.9871
1×10^4	29.60	84.32	35.564109	0.9871
1×10^5	29.60	84.32	35.564109	0.9871
1×10^6	29.60	84.32	35.564109	0.9871
1×10^7	29.60	84.32	35.564109	0.9871

Table 5. Optimized Parameters of Defect Density

parameters	value
defect type	neutral
capture cross section electrons (cm^2)	1×10^{-19}
capture cross section holes (cm^2)	1×10^{-19}
energetic distribution	single
reference for defect energy level Et	above the highest EV
energy with respect to Reference (eV)	0.6

open-circuit voltage (V_{oc}), short-circuit current density (J_{sc}), fill factor (FF), and power conversion efficiency (PCE) of each solar cell device.

The influence of the shunt resistance (R_s) was most pronounced at a value of $10 \Omega\cdot\text{cm}^2$. At this specific resistance value, the solar cell exhibited an efficiency of 3.16%,

accompanied by a fill factor of 25%, the short-circuit current density (J_{sc}) was measured at $35.56 \text{ mA}/\text{cm}^2$, and the open-circuit voltage (V_{oc}) stood at 0.5 V.

Subsequent to this particular point and for shunt resistance values ranging from $103 \Omega\cdot\text{cm}^2$ to $10^7 \Omega\cdot\text{cm}^2$, the parameters of efficiency, fill factor, J_{sc} , and V_{oc} remained constant. In other words, altering the shunt resistance within this range did not yield any appreciable changes in the performance characteristics.

3.7. Effect of the Interface Defect Density. The holes and electron carriers generated by light must pass through the interface to reach each electrode (it should be noted that the Auger recombination coefficient for the electron and the holes between the aluminum and CsPbI_3 are shown in Table 2). Also the interface defect density is important for device performance. The effects of the CsPbI_3/Al interface defect density were investigated in the interface defect density range of 10^8 to 10^{15} cm^{-3} .

Figure 9a,b shows the PCE, FF, J_{sc} , and V_{oc} curves in terms of total defect density, and (c) illustrates the current density–voltage (J – V) curves for the CsPbI_3/Al interfaces. Table 5 also shows the main variables used in the simulation: the performance of the device, in terms of PCE, FF, J_{sc} , and V_{oc} , remains stable despite changes in interface defect density within the tested range. This stability could be attributed to the compatibility between the CsPbI_3 and Al interface, indicating that within the specified range of interface defect densities, the device's performance is robust and not heavily impacted by changes in defect density and the materials can tolerate a certain level of interface defects without significantly compromising device performance.

3.8. Comparison of SCAPS-1D Results with Previous Work. Table 6 provides a comparative analysis between our results with the current theoretical and experimental research with different configurations devices. In comparison with all of the previous simulation results, all of the studied device performances were significant, and we have revealed the maximum PCE of 33.32–38.93%, which may help to identify more effective configurations for the near future.

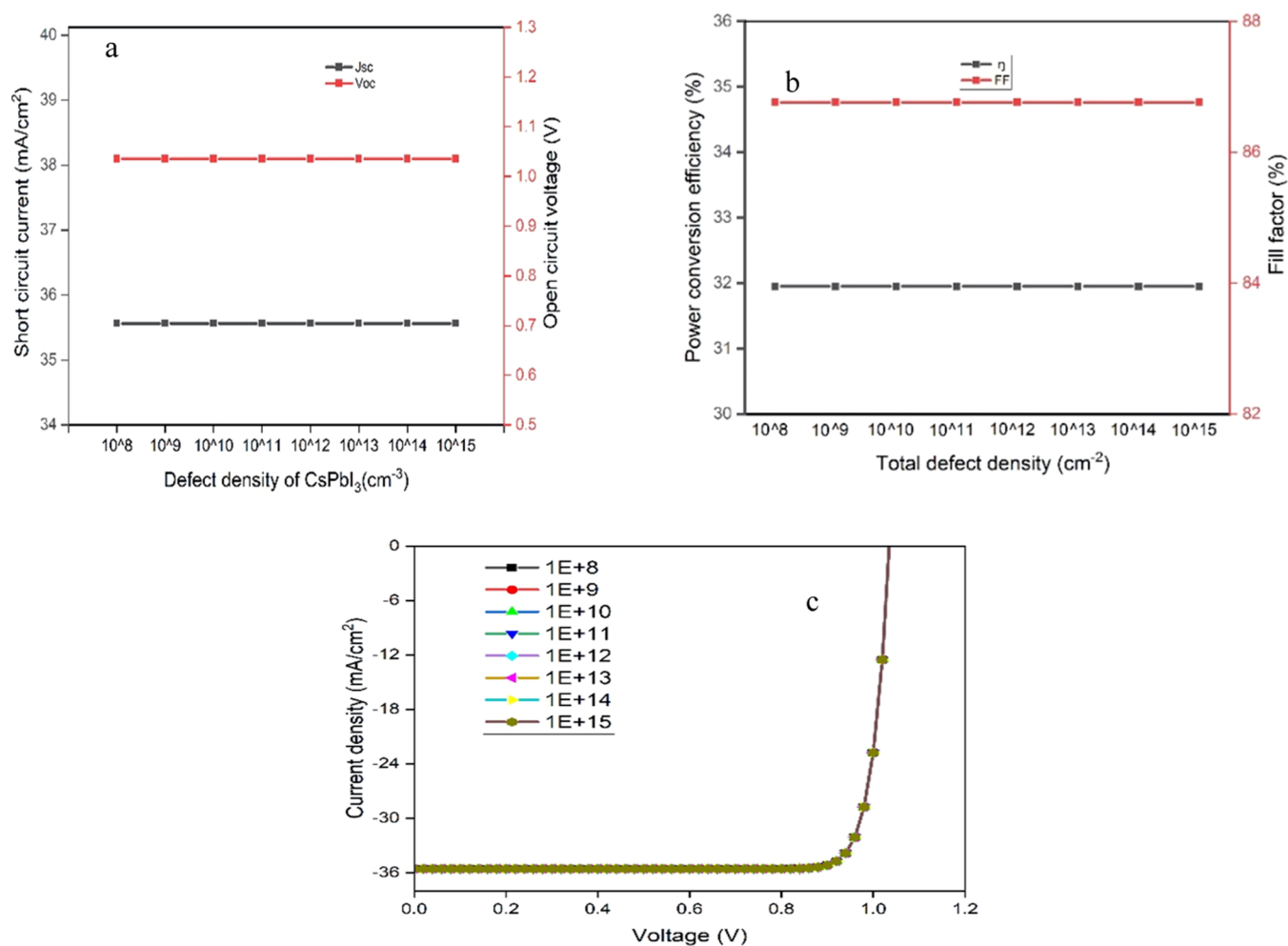


Figure 9. (a, b) PCE, FF, J_{sc} , and V_{oc} curves in terms of total defect density interface and (c) the current density–voltage (J – V) curves for the CsPbI_3/Al interfaces.

Table 6. Comparison of PV Parameters of Different Compositions of Heterojunction Structure Solar Cells

optimized devices	V_{oc} (mV)	J_{sc} (mA/cm^2)	FF (%)	PCE (%)	refs
$\text{TiO}_2(100 \text{ nm})/\text{i-CH}_3\text{NH}_3\text{SnBr}_3(15 \mu\text{m})/\text{CsPbI}_3(1 \mu\text{m})/\text{Al(BSF)}(50 \text{ nm})$	1.21	35.63	89.84	38.93	this work
$\text{ITO}(70 \text{ nm})/\text{n+c-Si}(1 \mu\text{m})/\text{p-c-Si}(150 \mu\text{m})/\text{MoOx}/\text{Ag}$	560.4	34.4	76.3	14.7	31
$\text{ZnO}(80 \text{ nm})/\text{a-Si:H}(5-10 \text{ nm})/\text{n a-Si:H}(3-5 \text{ nm})/\text{i-c-Si}(300 \mu\text{m})/\text{Al (BSF)}$	667.4	35.06	83.78	23.78	24
$\text{ITO}/\text{TiO}_2/\text{CH}_3\text{NH}_3\text{SnBr}_3/\text{NiO}$	0.8	31.88	84.89	21.66	17
$\text{ITO}(0.5 \mu\text{m})/\text{TiO}_2(0.4 \mu\text{m})/\text{CsPbI}_3(1.05 \mu\text{m})/\text{CBTS}(0.1 \mu\text{m})/\text{Au}$	0.98	21.1	85.39	18.06	32
$\text{ITO}(0.5 \mu\text{m})/\text{TiO}_2(0, \mu\text{m})/\text{CsPbI}_3(2.4 \mu\text{m})/\text{CBTS}(0.5 \mu\text{m})/\text{Ni}$	0.98	22	85.1	18	33
$\text{ITO}/\text{n-TiO}_2(0.0 \mu\text{m})/\text{Cs}_2\text{TiI}_6(4.33 \mu\text{m})/\text{p-CdTe}(2.75 \mu\text{m})/\text{Au}$	1.39	25.1	43.03	15.04	34
$\text{TiO}_2/\text{DSSCs}(12 \mu\text{m})$	17.6	0.76	70	9.52	35
$\text{Glass}/\text{SnO}_2: \text{F}/\text{SnO}_2/\text{CdS}/\text{CdTe}/\text{ZnTe}: \text{Cu}/\text{Au}$	0.794	25.19	69.36	13.87	36
$\text{FTO}/\text{TiO}_2/\text{CH}_3\text{NH}_3\text{PbI}_3/\text{carbon}$	1.08	25.33	79.27	21.64	18
$\text{Al}/\text{ITO}/\text{TiO}_2/\text{MoS}_2/\text{Ni}$	0.793	30.89	80.62	22.30	37
$\text{Al}/\text{ITO}/\text{TiO}_2/\text{MoS}_2/\text{In}_2\text{Te}_3/\text{Ni}$	1.084	37.22	82.58	33.32	37
$\text{ITO}/\text{PCBM}/\text{CsSnI}_3/\text{CuI}/\text{Au}$	0.91	14.24	78.11	10.10	38
$\text{ITO}/\text{Spiro-OMeTAD}/\text{CsPbI}_3$	1.152	17.71	76.56	15.62	39
$\text{Cu}_2\text{O}/\text{i-CH}_3\text{NH}_3\text{SnBr } 3/\text{TiO}_2$	0.93	33.89	80.23	25.52	40

4. CONCLUSIONS

This paper presents an analysis of $\text{TiO}_2/\text{i-CH}_3\text{NH}_3\text{SnBr}_3/\text{CsPbI}_3/\text{Al(BSF)}$ heterojunction solar cells, which were optimized by using the SCAPS-1D software package. The findings indicate that the performance of the solar cells improves with an optimized absorber thickness of $1.0 \mu\text{m}$ and a preamble layer with a thickness of $15.0 \mu\text{m}$. Upon optimization of these

parameters, the resulting cell exhibited a power conversion efficiency (PCE) of 38.93% and a fill factor (FF) of 89.84% with an acceptor concentration (N_a) at 10^{19} cm^{-3} and donor concentration (N_D) at 10^{16} cm^{-3} . The effects of the CsPbI_3/Al interface defect density were investigated in the interface defect density range of 10^8 – 10^{15} cm^{-3} . These simulation results

demonstrate the enhanced performance of $i\text{-CH}_3\text{NH}_3\text{SnBr}_3$ as a preamble layer in CsPbI_3 -based inorganic perovskite solar cells.

AUTHOR INFORMATION

Corresponding Author

Amina Arrar – Department of physics, Faculty of Technology, University of Relizane, BP 48000 W. Relizane, Algeria; Laboratory of Physics Thin Layer & Advanced Technologies, University of Relizane, BP 48000 W. Relizane, Algeria; orcid.org/0000-0002-3920-1411; Email: amina.arrar@univ-relizane.dz

Authors

Mohamed Ghaleb – Department of physics, Faculty of Technology, University of Relizane, BP 48000 W. Relizane, Algeria; Laboratory of Physics Thin Layer & Advanced Technologies, University of Relizane, BP 48000 W. Relizane, Algeria

Zaza Touaa – Department of physics, Faculty of Technology, University of Relizane, BP 48000 W. Relizane, Algeria; Laboratory of Physics Thin Layer & Advanced Technologies, University of Relizane, BP 48000 W. Relizane, Algeria

Complete contact information is available at:

<https://pubs.acs.org/10.1021/acsomega.3c03891>

Author Contributions

For research articles with several authors.

Notes

The authors declare no competing financial interest.

ACKNOWLEDGMENTS

The authors are grateful to University of RELIZANE for supporting this work, which is included in project of PRFU N° B00L02UN480120220002. Furthermore, the first author gratefully acknowledges Prof. Marc Burgelman, University of Ghent, Belgium for providing the SCAPS-1D simulate on software.

REFERENCES

- (1) Grace, T.; Yu, L.; Gibson, C.; et al. Investigating the effect of carbon nanotube diameter and wall number in carbon nanotube/silicon heterojunction solar cells. *J. Nanomater.* **2016**, *6* (3), No. 52.
- (2) Shockley, W.; Queisser, H. J. Detailed balance limit of efficiency of p - n junction solar cells. *J. Appl. Phys.* **1961**, *32* (3), 510–519.
- (3) Snaith, H. J. Perovskites: The emergence of a new era for low-cost, high-efficiency solar cells. *J. Phys. Chem. Lett.* **2013**, *4* (21), 3623–3630.
- (4) Yang, W. S.; Park, B. W.; Jung, E. H.; et al. Iodide management in formamidinium-lead-halide-based perovskite layers for efficient solar cells. *Science* **2017**, *356* (6345), 1376–1379.
- (5) Li, Z.; Zhao, Y.; Wang, X.; Sun, Y.; Zhao, Z.; Li, Y.; Zhou, H.; Chen, Q. Cost Analysis of Perovskite Tandem photovoltaics. *Joule* **2018**, *2* (8), 1559–1572.
- (6) Kojima, A.; Teshima, K.; Shirai, Y.; Miyasaka. Organometal halide perovskites as visible-light sensitizers for photovoltaic cells. *J. Am. Chem. Soc.* **2009**, *131* (17), 6050–6051.
- (7) Zhou, Y.; Zhu, K. Perovskite Solar Cells Shine in the “Valley of the Sun”. *ACS Energy Lett.* **2016**, *1* (1), 64–67.
- (8) Frolova, L. A.; Anokhin, D. V.; Piryazev, A. A.; Luchkin, S. Y.; Dremova, N. N.; Stevenson, K. J.; Troshin, P. A. Highly Efficient All-Inorganic Planar Heterojunction Perovskite Solar Cells Produced by Thermal Coevaporation of CsI and PbI_2 . *J. Phys. Chem. Lett.* **2017**, *8*, 67–72.
- (9) Masood, M. T.; Qudsiya, S.; Hadadian, M.; Weinberger, C.; Nyman, M.; Ahläng, C.; Dahlström, S.; Liu, M.; Vivo, P.; Österbacka, R.; Smått, J.-H. Investigation of Well-Defined Pinholes in TiO_2

Electron Selective Layers Used in Planar Heterojunction Perovskite Solar Cells. *Nanomaterials* **2020**, *10*, 181.

(10) Eperon, G. E.; Stranks, S. D.; Menelaou, C.; et al. Formamidinium lead trihalide: a broadly tunable perovskite for efficient planar heterojunction solar cells. *Energy Environ. Sci.* **2014**, *7*, 982–988.

(11) Chen, K. Q.; Zhong, Q. H.; Chen, W.; Sang, B. H.; Wang, Y. W.; Yang, T. Q.; Liu, Y. L.; Zhang, Y. P. Short-chain ligand-passivated stable α - CsPbI_3 quantum dot for all-inorganic perovskite. *Sol. Cells* **2019**, *29*, No. 1900991.

(12) Eperon, G. E.; Paternò, G. M.; Sutton, R. J.; Zampetti, A.; Haghghirad, A. A.; Cacialli, F.; Snaith, H. J. Inorganic cesium lead iodide perovskite solar cells. *J. Mater. Chem.* **2015**, *3*, 19688–19695.

(13) Wang, Y.; Liu, X.; Zhang, T.; Wang, X.; Kan, M.; Shi, J.; Zhao, Y. The role of dimethylammonium iodine in CsPbI_3 perovskite fabrication: additive or dopant. *Angew. Chem.* **2019**, *131*, 16844–16849, DOI: [10.1002/ange.201910800](https://doi.org/10.1002/ange.201910800).

(14) Zhang, H.; Tian, Q.; Xiang, W.; Du, Y.; Wang, Z.; Liu, Y.; Liu, L.; Yang, T.; Wu, H.; Nie, T.; Huang, W.; Najar, A.; Liu, S. Tailored Cysteine-Derived Molecular Structures toward Efficient and Stable Inorganic Perovskite Solar Cells. *J. Adv. Mater.* **2023**, *35* (35), No. e2301140, DOI: [10.1002/adma.202301140](https://doi.org/10.1002/adma.202301140).

(15) Tan, B.; Wu, Y. Dye-sensitized solar cells based on Anatase TiO_2 nanoparticle/nanowire composites. *J. Phys. Chem. B* **2006**, *110* (32), 15932–15938.

(16) Lee, B. H.; Song, M. Y.; Jang, S. Y.; Jo, S. M.; Kwak, S. Y.; Kim, D. Y. Charge transport characteristics of high efficiency dye-sensitized solar cells based on electrospun TiO_2 nanorod photoelectrodes. *J. Phys. Chem. C* **2009**, *113* (51), 21453–21457.

(17) Samiul Islam, M.; Sobayel, K.; Al-Kahtani, A.; Islam, M. A.; et al. Defect Study and Modelling of SnX_3 -Based Perovskite Solar Cells with SCAPS-1D. *Nanomaterials* **2021**, *11* (5), 1218.

(18) Duan, Q.; Ji, J.; Hong, X.; Fu, Y.; Wang, C.; Zhou, K.; Liua, X.; Yang, H.; Wang, Z.-Y. Design of hole-transport-material free $\text{CH}_3\text{NH}_3\text{PbI}_3/\text{CsSnI}_3$ all-perovskite heterojunction efficient solar cells by device simulation. *Sol. Energy* **2020**, *201*, 555–560.

(19) Burgelman, M.; Nollet, P.; Degraeve, S. In *Modelling Polycrystalline Semiconductor Solar Cells, Thin Solid Films*, 23rd European Photovoltaic Solar Energy Conference, Valencia, 2000; Vol. 361, pp 527–532.

(20) Saleh, A. N. Simulation and improvement the solar cell $\text{Cu}_2\text{CdSnS}_4$ and study the effect of absorption layer defect. *Turk. J. Comput. Math. Educ.* **2021**, *12* (13), 2765–2773.

(21) Moorthy, V. M.; Srivastava, V. M. Device Modelling and Optimization of Nanomaterial-Based Planar Heterojunction Solar Cell (by Varying the Device Dimensions and Material Parameters). *Nanomaterials* **2022**, *12* (17), 3031 DOI: [10.3390/nano12173031](https://doi.org/10.3390/nano12173031).

(22) Karimi, E.; Ghorashi, S. M. B. Simulation of perovskite solar cell with P 3 HT hole-transporting materials. *J. Nanophotonics* **2017**, *11* (3), No. 032510.

(23) Usha, M.; Vedanayakam, S. V.; Thyagarajan, K. Simulation and analysis of lead based perovskite solar cell using SCAPS-1D. *Indian J. Sci. Technol.* **2017**, *11* (10), 1–8.

(24) Naceur, S.; Chekneane, A.; Aillerie, M.; Hilal, H. S. Effect of ZnO-based TCO on the performance of a-Si H(n)/a-Si H(i)/c-SiH(p)/Al BSF(p+)/Al heterojunction solar cells. *Environ. Prog. Sustainable Energy* **2020**, *384* 13114. DOI: [10.1002/ep.13114](https://doi.org/10.1002/ep.13114).

(25) Deepthi Jayan, K.; Sebastian, V.; Kurian, J. Simulation and optimization studies on CsPbI_3 based inorganic perovskite solar cells. *Sol. Energy* **2021**, *221*, 99–108.

(26) Lin, L.; Jiang, L.; Li, P.; Xiong, H.; Kang, Z.; Fan, B.; Qiu, Y. Simulated development and optimized performance of CsPbI_3 based allinorganic perovskite solar cells,(2020), University, Fuzhou 350108, China *Solar Energy*, 198 454 460 DOI: [10.1016/j.solener.2020.01.081](https://doi.org/10.1016/j.solener.2020.01.081).

(27) Azri, F.; Meftah, A.; Sengouga, N.; Meftah, A. Electron and hole transport layers optimization by numerical simulation of a perovskite solar cell. *Sol. Energy* **2019**, *181* (181), 372–378.

(28) Usha, M.; Vedanayakam, S. V.; Thyagarajan, K. Simulation and analysis of lead based perovskite solar cell using SCAPS-1D. *Indian J.*

Sci. Technol. **2017b**, *10* (11), 1–8, DOI: 10.17485/ijst/2017/v11i10/110721.

(29) Babu, B. J.; Mandadapu, U.; Vedanayakam, S. V.; Thyagarajan, K. Optimisation of high efficiency tin halide perovskite solar cells using SCAPS-1D. *Int. J. Simul. Proc. Model* **2018**, *13* (3), 221.

(30) Dhass, A. D.; Natarajan, E. Influence of Shunt Resistance on the Performance of Solar Photovoltaic Cell, 978-1-4673-4634-4/.

(31) Mehmood, H.; Nasser, H.; Tauqeer, T.; Turan, R. *Numerical Analysis Of Silicon Heterojunction Solar Cell Based On Molybdenum Oxide As A Back Surface Field (Bsf)*, 33rd European Photovoltaic Solar Energy Conference and Exhibition, 2017.

(32) Hossain, M. K.; Rubel, M. H. K.; Toki, G. F. I.; Alam, I.; Rahman, Md. F.; Bencherif, H. Effect of Various Electron and Hole Transport Layers on the Performance of CsPbI₃-Based Perovskite Solar Cells: A Numerical Investigation in DFT, SCAPS-1D, and wxAMPS Frameworks *ACS Omega*, *7* 4743210 43230 DOI: 10.1021/acsomega.2c05912.

(33) Khalid Hossain, M.; Toki, G. F. I.; Alam, I.; Pandey, R.; Samajdar, D. P.; Rahman, Md. F.; Islam, Md. R.; Rubel, M. H. K.; Bencherif, H.; Madan, J.; Mohammed, M.K.A. Numerical simulation and optimization of a CsPbI₃-based perovskite solar cell to enhance the power conversion efficiency, *New Journal of Chemistry*. *New J. Chem.* **2023**, *47*, 4801–4817, DOI: 10.1039/D3NJ90126B.

(34) Ahmad, O.; Rashid, A.; Ahmed, M. W.; Nasir, M. F.; Qasim, I. Performance evaluation of Au/p-CdTe/Cs₂TiI₆/n-TiO₂/ITO solar cell using SCAPS-1D. *Opt. Mater.* **2021**, *117*, No. 111105, DOI: 10.1016/j.optmat.2021.111105.

(35) Lee, B. H.; Song, M. Y.; Jang, S.-Y.; Jo, S. M.; Kwak, S.-Y.; Kim, D. Y. Charge Transport Characteristics of High Efficiency Dye-Sensitized Solar Cells Based on Electrospun TiO₂ Nanorod Photoelectrodes. *J. Phys. Chem. C* **2009**, *113* (51), 21453–21457, DOI: 10.1021/jp907855x.

(36) Jiang, Y.; Hu, D.; Tang, P.; Zhang, J.; Liu, C.; Wang, W.; Zeng, G.; Wu, L.; Li, W.; Feng, L. A study of apparent quantum efficiency in different structures of cadmium telluride solar cells. *Sol. Energy* **2017**, *149*, 323–331, DOI: 10.1016/j.solener.2017.03.085.

(37) Ali, M. H.; Al Mamun, M. A.; Haque, M. D.; Rahman, M. F.; Hossain, M. K.; Md Touhidul Islam, A. Z. Performance Enhancement of an MoS₂-Based Heterojunction Solar Cell with an In₂Te₃ Back Surface Field: A Numerical Simulation Approach. *ACS Omega* **2023**, *8* (7), 7017–7029, DOI: 10.1021/acsomega.2c07846.

(38) Hossain, M. K.; Toki, G. I.; Samajdar, D. P.; Mushtaq, M.; Rubel, M. H. K.; Pandey, R.; Madan, J.; Mohammed, M. K.; Islam, M. R.; Rahman, M. F.; Bencherif, H. Deep Insights into the Coupled Optoelectronic and Photovoltaic Analysis of Lead-Free CsSnI₃ Perovskite-Based Solar Cell Using DFT Calculations and SCAPS-1D Simulations. *ACS Omega* **2023**, *8* (25), 22466–22485, DOI: 10.1021/acsomega.3c00306.

(39) Duan, L.; Zhang, H.; Liu, M.; Grätzel, M.; Luo, J. Phase-Pure γ -CsPbI₃ for Efficient Inorganic Perovskite Solar Cells. *ACS Energy Lett.* **2022**, *7* (9), 2911–2918.

(40) Akter, O.; Alam, M. S. In *An Efficient Lead-free SnBr₃ based Perovskite Solar Cell: Design and Optimization using SCAPS-1D*, 4th International Conference on Sustainable Technologies for Industry 4.0 (STI), 2022, 23001793.